International Journal of Nanomedicine

Dovepress
open access to scientific and medical research

Open Access Full Text Article

ORIGINAL RESEARCH

Zeolitic Imidazolate Framework (ZIF-8) Decorated Iron Oxide Nanoparticles Loaded Doxorubicin Hydrochloride for Osteosarcoma Treatment - in vitro and in vivo Preclinical Studies

Wenbo Wu[1,*], Xiaoli Yu[2,*], Jiaxiang Sun[3], Yuanyuan Han[3], Yuanye Ma[1], Guoqing Zhang[1], Qingming Ma[4], Qiang Li[3], Hongfei Xiang[1]

[1]Department of Orthopedics, the Affiliated Hospital of Qingdao University, Qingdao, 266003, People's Republic of China; [2]Department of Anesthesiology, the Affiliated Hospital of Qingdao University, Qingdao, 266100, People's Republic of China; [3]College of Physics, Center for Marine Observation and Communications, Qingdao University, Qingdao, 266021, People's Republic of China; [4]Department of Pharmaceutics, School of Pharmacy, Qingdao University, Qingdao, 266021, People's Republic of China

*These authors contributed equally to this work

Correspondence: Hongfei Xiang; Qingming Ma, Tel +86-532-61807860, Email xianghf@qdu.edu.cn; qma@qdu.edu.cn

Background: As a broad-spectrum antitumorigenic agent, doxorubicin (DOX) is commonly used as a chemotherapeutic drug for treating osteosarcoma (OS). Still, it is associated with significant cell toxicity and ineffective drug delivery, whereas the zeolite imidazolate framework is extensively applied in the biomedical field as a carrier owing to its favorable biocompatibility, high porosity, and pH-responsiveness. Therefore, we need to develop a drug delivery platform that can effectively increase the antitumorigenic effect of the loaded drug and concurrently minimize drug toxicity.

Methods: In this study, a Fe_3O_4@ZIF-8 nanocomposite carrier was prepared with ZIF-8 as the shell and encapsulated with Fe3O4 by loading DOX to form DOX- Fe_3O_4@ZIF-8 (DFZ) drug-loaded magnetic nanoparticles. Then, we characterized and analyzed the morphology, particle size, and characteristics of Fe_3O_4@ZIF-8 and DFZ by TEM, SEM, and Malvern. Moreover, we examined the inhibitory effects of DFZ in vitro and in vivo. Meanwhile, we established a tumor-bearing mouse model, evaluating its tumor-targeting by external magnetic field guidance.

Results: DFZ nanoparticles possessed have a size of ~110 nm, with an encapsulation rate of 21% and pH responsiveness. DFZ exerted a superior cytostatic effect and apoptosis rate on K7M2 cells in vitro compared to DOX($p<0.01$). In animal experiments, DFZ offers up to 67% tumor inhibition and has shown a superior ability to induce apoptosis than DOX alone in TUNEL results($p<0.01$). Tumor-targeting experiments have validated that DFZ can be effectively accumulated in the tumor tissue and enhance anticancer performance.

Conclusion: In summary, the DFZ nano-delivery system exhibited a more substantial anti-tumorigenic effect as well as superior active tumor targeting of DOX- Fe_3O_4@ZIF-8 compared to that of DOX alone in terms of biocompatibility, drug loading capacity, pH-responsiveness, tumor-targeting, and anti-tumorigenic effect, indicating its chemotherapeutic application potential.

Keywords: osteosarcoma chemotherapy, zeolite imidazolate framework, PH-responsive, nanocarriers, tumor targeting

Introduction

As is well documented, osteosarcoma, also referred to as osteogenic sarcoma, is the most prevalent native bone cancer in children and adolescents,[1,2] with localized pain and swelling as chief symptoms. Its primary clinical treatment is divided into three parts: preoperative neoadjuvant chemotherapy, surgical treatment, and postoperative chemotherapy.[3,4] Current chemotherapy modalities for osteosarcoma are predominantly Adriamycin-based regimens,[5] generally used in conjunction with methotrexate in neoadjuvant therapy, cisplatin, and postoperative adjuvant chemotherapy for the preoperative control of the primary focus,[6,7] thereby elevating the success rate of

Received: 3 October 2023
Accepted: 20 December 2023
Published: 28 December 2023

surgery and eliminating residual tumor cells postoperatively to mitigate the risk of metastasis. These chemotherapeutic agents are typically accompanied by side effects such as gastrointestinal reactions, hepatic impairment, cardiotoxicity, and bone marrow suppression.[8] In addition to the development of resistance to chemotherapeutic agents,[1] numerous acute and chronic side effects develop due to high doses of chemotherapy drugs and the high frequency of doses. Therefore, there is an urgent need to identify novel therapeutic strategies to improve chemotherapy outcomes in osteosarcoma patients and prolong their life expectancy. At present, nanocarriers provide a suitable platform for drug delivery, and their development has overcome the limitations of free therapies, drugs can cross systemic, microenvironmental, and cellular biological barriers.[9] Interestingly, multiple nanomaterials can serve as drug carriers, such as nanogels,[10,11] exosomes,[12] liposomes,[13] and molecular sieves;[14] those nanocarriers often have favorable biocompatibility and degradability and extend blood circulation time and consequently increase drug concentration in the blood owing to the high permeability and retention of tumor tissues. They also target selected tumor tissue receptors for precise treatment,[15–17] whilst nanocarrier particles lower the frequency and dose of drugs and enhance the effect of the loaded drug through the effects mentioned above.

Among these materials, metal-organic frameworks (MOFs) are an emerging class of heterogeneous porous materials comprising metal ions or metal clusters bridged by organic ligands, possessing high porosity, tunable size, high loading, thermal stability, good biodegradability, and biocompatibility,[18,19] which naturally are widely used in the biomedical field.[20–23] Zeolitic Imidazole Frameworks (ZIFs), ZIF-8, among the MOFs, is frequently used as a carrier for drug delivery with negligible cytotoxicity and pH sensitivity.[24–26] For example, intelligent nanoprobes consisting of lanthanide-doped nanoparticle (LTNP) cores and ZIF-8 are used for tumor drug resistance assessment.[27] Biomimetic ZIF-8 nano-systems with the ability to alleviate tumor hypoxia for enhanced chemical-photothermal synergistic antitumor. The DOX/BSA pH-responsive drug delivery system was constructed using ZIF-8 as a shell to encapsulate bovine serum albumin (BSA).[28]

In this paper, a more straightforward and greener fabrication method was used to synthesize Fe3O4,[29] after which 2-methylimidazole and zinc (molar ratio 8:1) nitrate were mixed to synthesize ZIF-8 by linking divalent metal cations to imidazole acid anions on a tetrahedral framework to form coordination bonds as Fe_3O_4 nanoparticle coatings to construct Fe_3O_4@ZIF-8 nanocarrier complexes eventually.[30] Overall, the Fe_3O_4@ZIF-8 nanocarrier has been consistently utilized as a purification material to treat hazardous substances in wastewater or chemical waste streams.[31–34] At the same time, other studies reported that the pH sensitivity of Fe_3O_4@ZIF-8 was used to carry norfloxacin to construct pH-responsive nanocarriers.[25,35] Sustained release microspheres of ropivacaine encapsulated in zeolite imidazole framework-8 (RVC@ZIF-8) have been synthesized for use in analgesic therapy.[36] It can be seen that Fe_3O_4@ZIF-8 composite nanomaterials possess both the desirable properties of MOF materials and the magnetic guidance of Fe3O4 nanoparticles, conferring Fe_3O_4@ZIF-8 carriers with magnetic targeting and magnetic separation properties[37,38] In this direction, due to the unique structure of ZIF-8 and the reactive characteristics[26,39] of the tumor microenvironment,[40,41] ZIF-8 has been used as a carrier for loading chemotherapeutic agents for cancer treatment.[42–48] Thus, we took this as a starting point to construct a magnetic nano-drug delivery system.

Herein, DFZ drug-loaded nanoparticles were prepared for the treatment of OS with DOX and Fe_3O_4@ZIF-8 nanocarriers, and their morphology, particle size, and composition were analyzed via TEM, SEM, XRD, and FR-IT. Additionally, their encapsulation rate, drug loading rate, and release characteristics were determined. In vitro cytotoxicity and cellular uptake, assays of Fe3O4@ZIF-8 were performed using K7M2 tumor cells to assess their biocompatibility. Cell counting kit 8, inverted fluorescence microscopy, and flow cytometry assays were also used to compare the cytotoxicity and drug uptake of free DOX and DFZ on osteosarcoma cell lines. Finally, an animal tumor model was established, and the tumor-targeting aggregation of DFZ, as well as a more substantial in vivo anti-tumorigenic effect compared to the chemotherapeutic agent alone, were demonstrated by the action of an applied magnetic field. Therefore, the study of this nano drug delivery platform with active targeting has broadened the approach for the treatment of osteosarcoma.

Materials and Methods

Materials and Reagents

All the cell-culture medium (DMEM), FBS, double antibodies (Penicillin-streptomycin solution), and phosphate-buffered saline (PBS) were bought from Qingdao Haosail Technology Co., Ltd, China. Zinc nitrate hexahydrate ($Zn(NO_3)_2 \cdot 6H_2O$,99%) and 2-methylimidazole ($C_4H_6N_2$,98%) were obtained from Aladdin Reagent Company (Shanghai, China). DAPI, Hoechst3334, Cell Counting Kit-8 (CCK-8), and Annexin V-FITC/PI Apoptosis Detection Kit were purchased from Beijing Solarbio Science and Technology Co., Ltd, China. TUNEL Kit was purchased from Sigma-Aldrich (St. Louis, MO, USA). All other chemical reagents in the study were confirmed as analytical grade.

Fabrication of Fe3O4@ZIF-8 and DOX-Fe3O4@ZIF-8

According to the literature, Fe_3O_4@ZIF-8 was synthesized using an optimized method reported in a previous study.[29] Briefly, 114 g of $FeCl_3$-$6H_2O$ and 2.4 g of sodium acetate with 0.65 g of sodium citrate were dissolved in a mixed solution of 37.5 mL of diethylene glycol and 12.5 mL of ethylene glycol, and the solution was magnetically stirred at room temperature for 2 h to become an orange-red transparent solution. Then, the solution was transferred to a Teflon-sealed autoclave heated at 200 °C for 10 h and cooled naturally to room temperature. The Fe304 nanoparticles were separated by a magnet and then washed with ethanol, followed by vacuum drying at 60°C for 24 h. The synthesis of Fe_3O_4@ZIF-8 was based on the conditions reported in the literature and optimized in steps.[36] In brief,50 mg of iron oxide nanoparticles was added to 100 mL of methanol solution, and the resulting mixture was sonicated for 30 min. Then, 4.1 g of 2-methylimidazole was dissolved in 50 mL of methanol, which was subsequently slowly poured into the above solution, followed by sonication for 15 min. Next, 1.86 g of zinc nitrate was added to 50 mL of methanol solution and mixed with the above solution, which was thereupon placed in a dry blast box at 25 °C. The solution was stirred at 5 min intervals until homogeneous and then left to react for 1 h. The solid precipitate was acquired by magnetic separation, washed with methanol, magnetically separated three times to remove excess ZIF-8, and finally centrifuged to obtain Fe3O4@ZIF-8 nanoparticles. Finally, the resulting substance was vacuum-dried for 24 h at 60 °C and stored for the ensuing experiments.

Characterization of Fe_3O_4@ZIF-8 and DOX- Fe_3O_4@ZIF-8

The morphology and structure of Fe_3O_4@ZIF-8 and DOX- Fe3O4@ZIF-8 were observed by transmission electron microscopy (TEM, OLYMPUS, Japan) and scanning electron microscopy (SEM, JSM-6309LV, Japan), and particle size distribution was analyzed in triplicate by Malvern Zeta size NanoZS90 at 25°C, scattering Angle 90°(British Malvern Instrument Co. Ltd, UK). The composition was determined by X-ray diffraction of the samples (PXRD, Malvern Nano ZS, UK), and the samples were characterized by Fourier infrared spectrometer 9 from Bruker (FT-IR), FTIR analyses were conducted in terms of DFZ at the speed of 2 mm/s by and in the range of 500–4000/cm (VERTEX 70, Broker, Germany). The loading efficiency and release rate were measured by UV-vis spectrophotometer (UH4150, Japan).

Drug Loading and Release of DOX- Fe_3O_4@ZIF-8 Nanoparticles

30 mg of Fe_3O_4@ZIF-8 was dissolved in 30 mL of deionized water and sonicated for 15 min. Then, 15 mg DOX was added, and the resulting solution was shaken at room temperature for 24 hours. After centrifugation (12,000 r, 10 min), the mixture was washed in 30 mL of deionized water. This process was performed in triplicate. The drug-loaded nanoparticles DOX- Fe_3O_4@ZIF-8 were obtained by vacuum drying at 60 °C for 24 h. To calculate the loading and encapsulation rates, aqueous solutions of 5–15 μg/L DOX were prepared to plot standard curves. The absorbance values in the supernatant were measured by a UV spectrophotometer at the maximum absorption wavelength of DOX (λ Max=480 nm) to determine the unloaded DOX mass, and the DOX mass in the drug-loaded particles (m1) was calculated as follows: encapsulated efficiency (EE %) = m1/m0*100% (1) drug loading efficiency (DL %) = m1/mt*100% (2) Where m0 represents the total drug weight, and mt stands for the weight of drug-laden nanoparticles.

The drug released from drug-loaded particles was measured in PBS solution at different PH. More specifically, 5 mg of DFZ was added to 5 mL of pH=7.2 and pH=5.0 PBS solution. The solution was separated, placed in an oscillator, and

gently shaken at 100 r/min. After magnetic separation of the solution at different time points, unloaded DOX in the supernatant was calculated by UV-Vis, the detection wavelength was 190–900 nm, and the drug accumulation and release rates were derived. Finally, 5 mL of PBS buffer was added to continue the drug release process, and the drug release profile was plotted.

Culture of Cells

The osteosarcoma cell line (K7M2) was purchased from the Chinese Academy of Sciences Cell Bank (Shanghai, China), this is a type of osteoblastoma. Osteosarcoma cells were cultured in a DMEM medium containing 10% fetal bovine serum (FBS) and 1% double antibodies (Penicillin-streptomycin solution). The cells were cultured in an incubator at 37 °C at atmospheric pressure and 5% CO2. The cells in the logarithmic growth stage were used for experimental studies.

In vitro Anti-Tumor Assay

To verify the ability of DFZ to inhibit tumor proliferation in vitro and whether nanocarrier Fe_3O_4@ZIF-8 is cytotoxic, we used the cell counting kit-8 (Solarbio, China) for this experiment according to the operating instructions. CCK8 kits can reduce exogenous 3–4,5-dimethyl-2- thiazolium−2,5-diphenyl−2-H-tetrazolium bromide (MTT) to Formazan. The absorbance value is measured on a microplate reader (Infinite M200 Pro, Swiss TECAN Company), which indirectly reflects the number of viable cells. K7M2 cells in the logarithmic growth phase were digested and collected to form cell suspension. Then, the cells were plated in 96-well plates at a density of 2000 cells per well. After 24 h of incubation, the medium was removed. 100 μL of the DFZ drug medium containing different gradient concentrations of DOX (1.0, 2.5, 5.0, 7.5, and 10.0ug/mL) was added to the 96-well plate as the experimental group, with free drug DOX acting as the drug group control (1.0, 2.5, 5.0, 7.5, and 10.0ug/mL) and blank medium as the empty group, the control group were the cells that did not receive any treatment. Afterward, 10 μL of cck8 reagent was added to each well after 24 h and 48 h of incubation, respectively. Optical density (OD) was measured at 450 nm. Tumor cells were also cultured at the same concentration gradient of the Fe3O4@ZIF-8 nanocarrier for 24 h and 48 h, and cell viability and biocompatibility were assessed.

Cell survival % = (OD drug group-OD blank group) / (OD control group-OD blank group)*100% (3).

In vitro Cell Uptake Experiment

The distribution of drugs in cells can be observed by an inverted fluorescence microscope (Nikon A1R MP, Japan). K7M2 cells were plated at a density of 5000 cells/300μL in 24-well plates, incubated for 24 h, and then incubated with DFZ drug-loaded nanoparticles for 2 h at 37 °C. Next, the cells were fixed with 4% paraformaldehyde at room temperature for 20 min, followed by washing with PBS three times for more than 5 min. Nuclei were stained with DAPI reagent for 15 min, aspirated, and added to PBS solution. The endocytosis of nanoparticles by tumor cells was observed under different magnifications of fluorescence microscope. Then, tumor cells were prepared using a similar approach by adding 300 μL of 10 μg/mL drug-laden nanoparticles drug medium. At the same time, the Fe_3O_4@ZIF-8 group and the free DOX group were cultured, and nuclear staining was likewise performed after 24 h and 48 h for visualization, which emitted blue fluorescence at a laser excitation wavelength of 405 nm and red autofluorescence at a laser excitation wavelength of 488 nm. DOX fluorescence intensity was quantified by Image J analysis (ImageJ, USA).

In vitro Apoptosis Assay

The effect of Fe_3O_4-ZIF-8 and DFZ on cell apoptosis of K7M2 cells was performed with the FITC/PI Apoptosis Detection Kit (HY-K-1073, MCE, US) according to the instruction. The cells were prepared as described above and inoculated into 6-well plates at a density of $1\times10^{\wedge6}$ cells/2mL per well in a 37 °C, 5% CO2 cell incubator for 24 h. The original medium was discarded after cell adhesion, and DFZ(DOX:10ug/mL) and free DOX (10ug/mL) drugs were added, respectively. The medium was used as a blank, and tumor cells were incubated for 24 h. Next, the K7M2 cells were stained by using the live/dead cell assay kit according to the manufacturer's instructions. Cells were resuspended by adding 500μL of diluted Binding Buffer. Add 5μL of Annexin V-FITC Reagent and 5μL of PI Reagent (50μg/mL) to the cell suspension, gently vortex and mix well, and incubate for 15~20 minutes at room temperature away from light. The

assay was performed immediately. Lastly, the cells were examined using a flow cytometer (BD AccuriC6, USA). (FITC ex/em:488/520 nm, PI ex/em:536/617 nm).

Establish the Experimental Mouse Model

All the experimental procedures have complied with protocols and guidelines approved by the Animal Management Rules of the Ministry of Health of the People's Republic of China (document No. 552001) and the examination and approval of the Laboratory Animal Welfare Ethics Committee of Qingdao University. Experimental animals were kept under a 12 h light 12 h dark cycle, were fed with a standard laboratory rodent diet, and were provided with tap water. BALB/c mice (female, 18–20 g, six to seven weeks old) were obtained by Jinan Pengyue Experiment Breeding Co., LTD. Mice were subcutaneously inoculated on the left flank with K7M2 cells ($10^{\wedge 8}$ cells, 100 μL) after preparing their skins. Tumor volume in mice was essentially up to 50 $mm^{\wedge 3}$ by the tenth day after the procedure. The tumor volumes were calculated according to the formula as Volume = (Length × $Width^{\wedge 2}$)/2.

Tumor Targeting Research

In this experiment, we used 5(6)-carboxy fluorescein (FAM) loaded in the nanocarrier Fe_3O_4@ZIF-8.To begin, FAM-Fe_3O_4@ZIF-8 was prepared by adding FAM into Fe_3O_4@ZIF-8 saline solution and stirred for 24 hours in the dark. The method mentioned above was used to establish the tumor model. Once the tumor reached a volume of 50 $mm^{\wedge 3}$, the drug was administered, and the animals were randomly assigned to two groups, each group containing 5 mice. The first group was guided by an external magnetic field, whereas the other group was not. Five animals were injected with 200 μL of FAM- Fe_3O_4@ZIF-8 (0.5mg/mL) in the tail vein. Mice in the experimental group were placed under a magnetic field (N52 Grade 10 mm ×10 mm × 2 mm, Pull Force: 3.3lb), whereas the control group was not. After FAM injection 3, 6, 12, 24, and 48 h, mice were photographed using the Filter Pair mode of an animal 3D imaging system (Perkin Elmer, USA). After 48 hours, the mice were euthanized under the Animal Management Rules of the Ministry of Health of the People's Republic of China, and organs (heart, liver, spleen, lungs, and kidneys) and tumor tissues were collected for imaging and quantitative analysis, stored in paraformaldehyde solution (4.0%), and washed twice with PBS to remove excess paraformaldehyde. An animal 3D imaging system was used to capture images and analyze dates (ImageJ, USA).

In vivo Anti-Tumor Experiment

After the tumor volume of the mice attained 50 $mm^{\wedge 3}$, mice were randomly divided into five groups receiving different treatments to assess the anti-tumor effect of DFZ in vivo: the saline control group was labeled G1, the nanocarrier Fe_3O_4@ZIF-8 group represented G2, the DOX group was G3, drug-carrying nanoparticles was G4 (DOX:5mg/kg), drug-carrying nanoparticles with the magnetic field was G5. Notably, the DOX dosage was 5 mg/kg. On days 0, 3, 6, 9, and 12 following model establishment, the mice were administered the designated drug. Mice in the G5 group were treated with magnetic guidance by placing a magnet at the tumor site within 48 h after drug injection(N52,10*10*2mm). At the same time, mice's body weight and tumor volume were measured and recorded at specific time points (10, 13, 16, 19, 22, 25, 28).

Mice were all sacrificed on day 18 after drug administration, and isolated tumors and major organs (heart, liver, spleen, lungs, and kidneys) were harvested and weighed with a microbalance. They were then fixed with 4% paraformaldehyde and washed twice with PBS to remove excess paraformaldehyde.

Immunohistochemical Evaluation

In this experiment, the major organ tissues and tumor tissues of treated mice were embedded in paraffin and finally cut into 7μm sections for histopathological analysis. Next, we monitored apoptosis in tumor tissue using the dUTP-labelled terminal deoxynucleotidyl transferase assay. Although this method can also label dead cells, mishandling the process can cause cell death and affect the results. In normal cells, however, DNA breaks are almost nonexistent, so the method accurately reflects true apoptosis and has better sensitivity than the general method. To detect the expression level of TUNEL apoptosis, we then stained major organs and tissues using the TUNEL method (50μL, 37°C, 1 h) according to the manufacturer's protocol (Roche).

Statistical Analysis

Statistical analysis of relevant data was performed using SPSS (version,25.0), and significance analysis was performed using descriptive statistics, and single-factor analyses of variance (ANOVA) followed post hoc Tukey test, All the data were represented as mean±standard deviation across three to five independent measurements. The Student's t-tests for comparisons among treatment groups. $P<0.05$ was considered a significant difference, and $P<0.01$ was regarded as a highly significant difference.

Results and Discussion

Characterization of Fe3O4@ZIF-8 and DOX-Fe3O4@ZIF-8

In the current paper, the synthesized Fe_3O_4@ZIF-8 and DFZ were analyzed by transmission electron microscopy, scanning electron microscopy, and a Malvern particle size analyzer for morphology, structure, and particle size. As illustrated in Figure 1A and D, nanocarriers Fe_3O_4@ZIF-8 are formed by wrapping Fe_3O_4 with ZIF-8, respectively, the forms of Fe_3O_4@ZIF-8 and DFZ nanocomposites possessed a shell-core structure. According to the results of scanning electron microscopy (Figure 1B and E), there are only some differences in the shape of Fe3O4@ZIF-8 and DFZ nanocomposites. The particle size distribution of Fe_3O_4@ZIF-8 and DFZ is shown in Figure 1C and F, the average diameter of Fe_3O_4@ZIF-8 and DFZ was 105±5.6nm and 110 ±10.3nm. In addition, the increase in particle size from nanocarriers to drug-loaded particles signaled the successful loading of chemotherapeutic drugs. The formation of the shell-core system was further validated by Fourier transform infrared spectroscopy

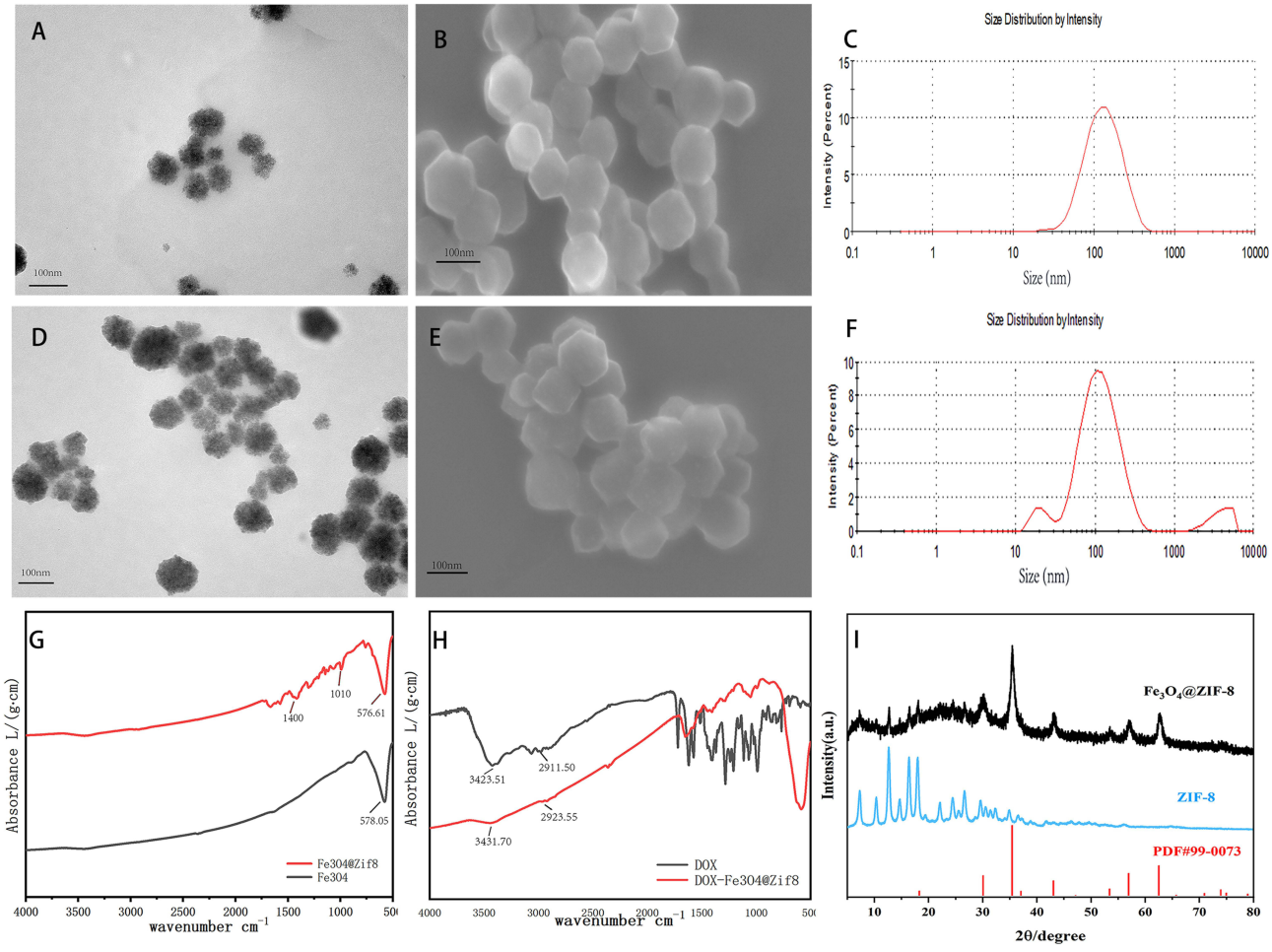

Figure 1 Characterization of Fe_3O_4@ZIF-8 and DFZ. (**A and D**) TEM images of Fe_3O_4@ZIF-8 and DFZ. (**B and E**) The SEM image of Fe_3O_4@ZIF-8 and DFZ. (**C and F**) Particle size distribution of Fe_3O_4@ZIF-8 and DFZ. (**G-H**) Fourier transform infrared spectroscopy (FTIR) analysis of the Fe_3O_4, Fe_3O_4-ZIF-8, free DOX, and DFZ. (**I**) X-ray diffraction (XRD) of Fe_3O_4@ZIF-8, the purified ZIF-8 and Fe3O4 standardized cards.

(FT-IR) and X-ray diffraction (XRD). In the XRD result plot (Figure 1I), the diffraction peaks at 12.72°, 16.50°, and 18.12° for @ZIF-8 were consistent with the crystallographic data of the prepared ZIF-8 control. The peaks at 30.49°, 56.97° and 62.71° for Fe3O4 and Fe_3O_4@ZIF-8 nanoparticles, respectively, were in agreement with the standard card Fe3O4 (PDF#99-0073) of the crystalline plane (220), (511), and (440) coincide. As displayed in Figure 1G, the characteristic absorption bands of Fe3O4@ZIF-8 were iconic Fe-O vibration peaks at 576.61 cm^{-1} owing to the stretching vibration of the amide bond in ZIF-8 at 1020–1400 cm^{-1}. These results confirmed the successful modification of Fe_3O_4 nanoparticles by ZIF-8. Within the results (Figure 1H), the characteristic peaks of DOX- Fe_3O_4@ZIF-8 at 3431.70.34 cm^{-1} and 2923.55 cm^{-1} reflected the O-H and N-H stretching vibrations of the hydroxyl and amino groups in DOX, suggesting that the DOX- Fe_3O_4@ZIF-8 nanoparticles were successfully prepared. The presence of such hydrophilic groups increases the stability of the composite nanoparticles in blood circulation and amplifies the EPR effect on the tumor tissue.[49,50]

The ability to target DFZ magnetic nanoparticles was demonstrated under the condition of the applied magnetic field, and the evidence was attached to the Supplementary File in the form of a video.

Determination of Drug Loading and Release of DOX- Fe_3O_4@ZIF-8

To determine the encapsulation efficiency and drug loading rate, 0–15 μg/L aqueous solution of Adriamycin hydrochloride was prepared to plot the standard curve (Figure 2A); the equation y=0.0159x+0.1342 was fitted to obtain a drug loading rate of 21% in 30 mL of aqueous solution containing 15 mg of DOX and 30 mg of Fe_3O_4@ZIF-8. The high drug loading rate was primarily attributed to the positive and negative electrostatic interaction between the carboxyl group and DOX and the formation of coordination bonds between zinc ions and DOX.[51] In addition, the in vitro release behavior of DOX- Fe_3O_4@ZIF-8 was explored in PBS buffer solutions of different PH. As depicted in Figure 2B, the initially rapid drug release from the surface of the nanoparticles was significantly dependent on pH, with release rates of 45.3% and 80.1% at 48 h, respectively. Due to the electrostatic interaction of DOX being disrupted after DFZ carboxyl protonation under acidic conditions, the coordination bonds between the imidazole group of ZIF-8 and zinc ions became unstable, causing faster drug release.[52] It is worthwhile emphasizing that DOX had higher solubility and a quicker release rate under acidic conditions, which promoted the release of DOX from Fe_3O_4@ZIF-8 into the solution and raised the release rate.[53] It has been reported in the literature that ZIF-8 exhibits pH-triggered controlled drug release properties when loaded with common chemotherapeutic agents such as 5-fluorouracil or doxorubicin.[39,54] Due to the significant differences in the pH of the microenvironment inside and outside tumor cells, drug-loaded nanoparticles can exhibit different release behaviors at these two locations, with a higher drug release rate inside tumor cells, resulting in greater anti-tumor activity.

DOX- Fe_3O_4@ZIF-8 in vitro Uptake Assay

Firstly, K7M2 tumor cells were incubated in a DFZ medium solution for 2 h. Then, the nuclei were stained using the intrinsic fluorescence of DOX, ie, red fluorescence and blue fluorescence for nuclei. Red fluorescence can be observed in osteosarcoma K7M2 cells after 2 h (Figure 2C and D). In contrast, black drug-loaded nanoparticles can be observed in nearby tumor cells, implying that drug-loaded nanoparticles were endocytosed into tumor cells, which in turn increased the local concentration of the drug and enhanced the tumor suppressive effect.

Furthermore, there was no significant difference in cell density in the blank and Fe_3O_4@ZIF-8 groups at 24 h and 48 h (Figure 2E and F), signifying that the Fe_3O_4@ZIF-8 nanocarriers possessed adequate biocompatibility. Contrastingly, the cell density in the DFZ group was significantly lower compared to that in the free DOX group, corroborating that the DFZ drug-loaded nanoparticles outperformed the DOX drug in terms of cell-killing effect, which was in line with the quantitative results of DOX fluorescence intensity delineated in Figure 2G.

In vitro Survival Rate Experiments of Fe3O4@ZIF-8 and DOX-Fe3O4@ZIF-8

The bio-toxicity of materials is quite often the most fundamental consideration in biomedicine. K7M2 osteosarcoma cells were cultured in different concentration gradients of Fe_3O_4@ZIF-8 nanoparticle medium solution (0,1.0,2.5,5.0,7.5,10.0 ug/mL) for 24 h and 48 h (Figure 3A and B). Cell viability was still 93.0% after 48 hours. The results inferred that the nanoparticle carrier had almost no cytotoxicity and was biocompatible. We next further validated the in vitro anti-tumor

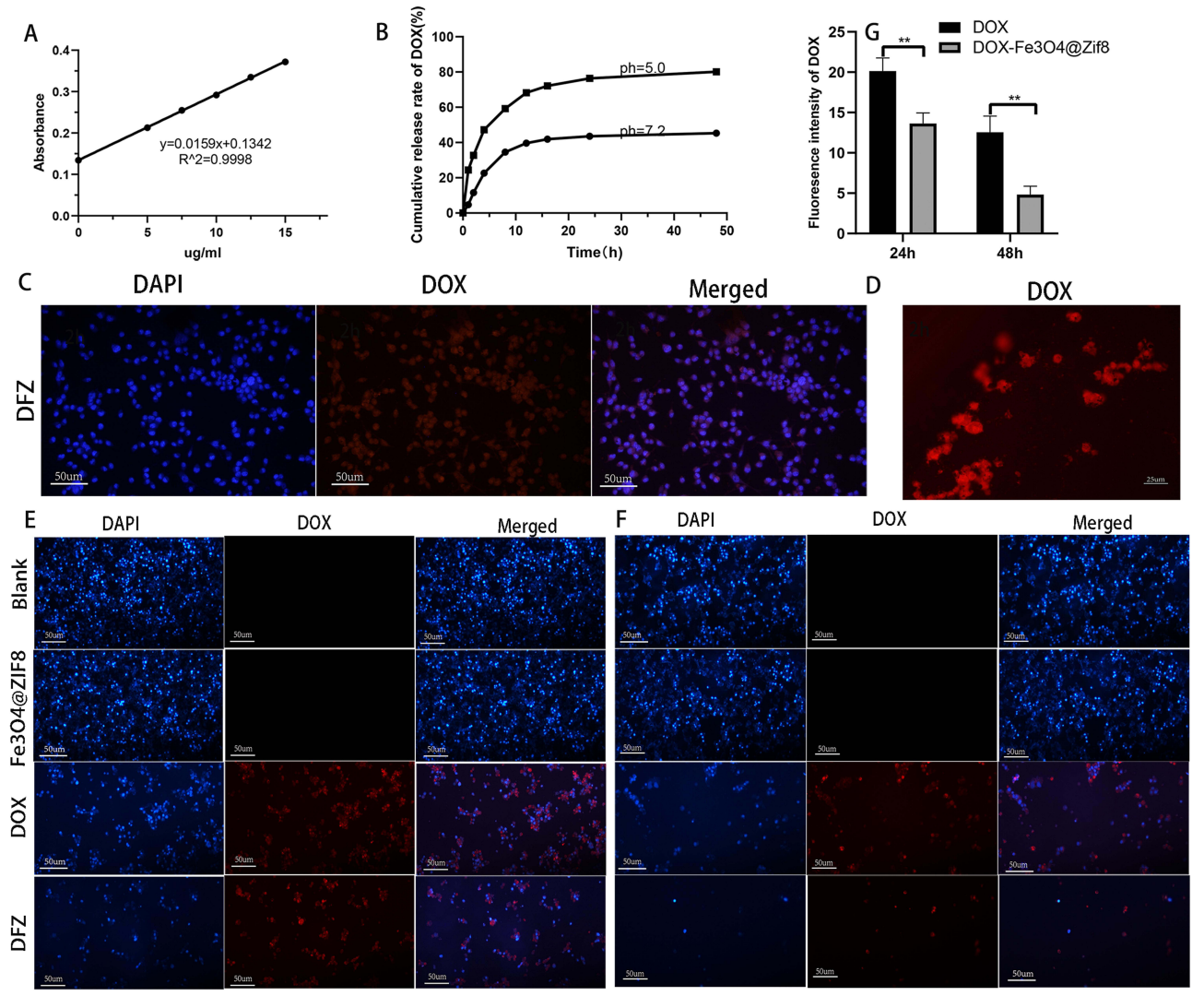

Figure 2 Characterization of DFZ. (**A**) The standard curves of DOX. (**B**) Cumulative DOX release from DFZ composites in different PBS buffers. (**C-D**) K7M2 tumor cells were treated by incubation with DOX-Fe3O4@ZIF-8 for 2 h with an inverted fluorescence microscope. (**E and F**) Inverted fluorescence microscope images of K7M2 tumor cells incubated with DOX and DFZ for 24h and 48h. (**G**) Fluorescence intensity of DOX with different treatments. **p < 0.01, n=3.

ability of DFZ. The DFZ NPs and DOX were incubated with cells for 24h and 48h at different DOX concentrations (1.0,2.5,5.0,7.5,10.0 ug/mL). As seen in Figure 3C and D, the DFZ nanoparticle and DOX both groups showed dose-dependent cytotoxicity. The cell survival rate was 19.61% and 39.61% at a DOX concentration of 10 μg/mL after 24 h of culture. It can be deduced that the inhibitory rate of cells in the DFZ experimental group was significantly higher than that in the free DOX control group. After 48 h, the majority of tumor cells in the experimental group were eliminated when the concentration of DOX was 10ug/mL, while the survival rate of the DOX group was 23.39%. Altogether, the above results were essentially attributed to the pH-responsive release of ZIF-8 nanomaterials in the acidic microenvironment of tumor cells. The endocytosis of drug-loaded nanoparticles by K7M2 cells, conjointly increased the intracellular concentration of DOX.[55] Similarly, Wang et al wrapped Cu^{2+} MOFs, which degraded and released Cu^{2+} and Zn^{2+} in the acidic environment of cellular lysosomes, resulting in a chain reaction to improve the efficacy of intracellular anticancer drugs.[56] This cck8 result shows that Fe_3O_4@ZIF-8 nanocarriers possessed excellent cytocompatibility and great potential for in vivo-based applications. DFZ has better tumor inhibition ability in vitro than DOX, which is consistent with the results of the cell uptake assay. For the commonly used MTT assay, the cck8 produces Formazan that is soluble in water and does not need to be dissolved in DMSO, which reduces toxicity to the cells, reduces the reproducibility of the experiments, and is more convenient to handle.

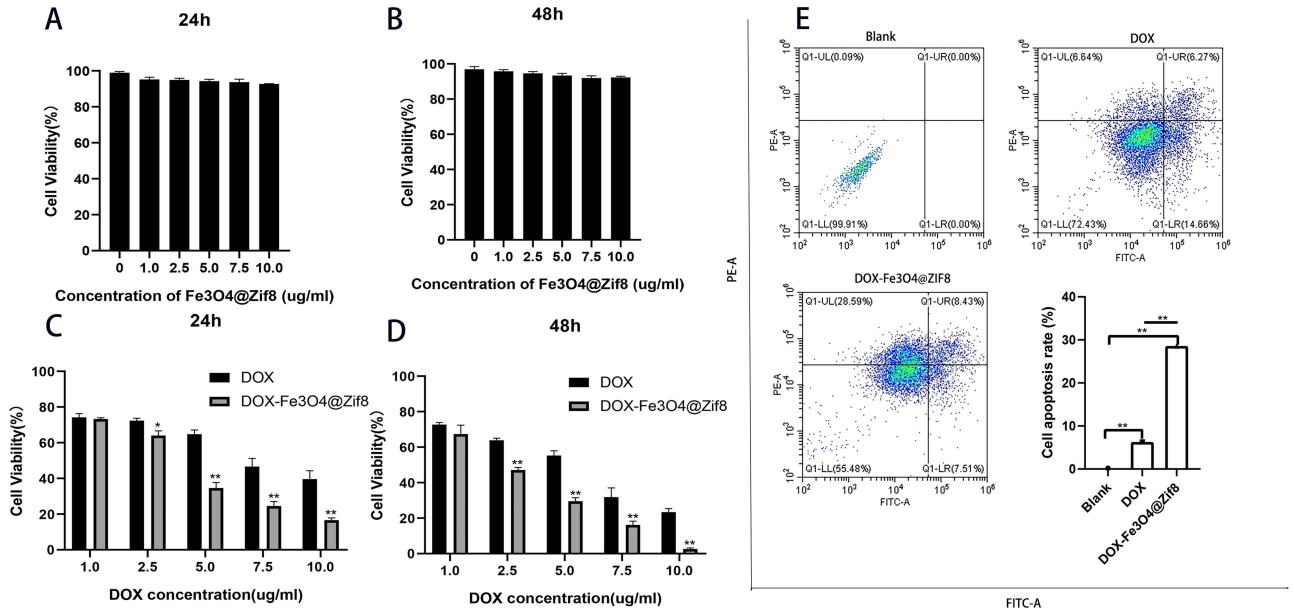

Figure 3 Cellular experiments with DFZ. (**A-D**) Cell viability of tumor cells incubated with different concentrations of Fe_3O_4-ZIF-8 (**A** and **B**), DOX, and DFZ (**C** and **D**) for 24 h and 48 h in pH 7.4 medium. (**E**) Cell apoptosis rate analysis experiment after incubating tumor cells with DOX and DFZ for 24h. Q1-UL: necrotic cells; Q1-UR: late apoptotic cells; Q1-LR: early apoptotic cells; Q1-LL: normal cells. The cells in the late stage of apoptosis were selected as apoptotic cells. The statistical data are represented as the mean ± SD. (Student's *t*-test; *p < 0.05, **p < 0.01, n=3).

Apoptotic Effect of DOX- Fe_3O_4@ZIF-8

In this experiment, the ability of DOX-Fe3O4@ZIF-8 drug-loaded nanoparticles and free DOX to induce apoptosis and kill K7M2 osteosarcoma cells was directly compared, and the cells were incubated with blank control, DFZ and DOX for 24 h in an incubator at 37 °C. As shown in Figure 3E, the apoptotic rate in the DFZ group of 37.02% was higher than the mortality rate of 12.91% in the free DOX group ($p < 0.01$), which agreed with the results of in vitro cell survival experiments. This result may be because the appropriate size of the DFZ is more likely to pass through the cell membrane, and also that the PH-responsiveness of ZIF-8[39] can increase the local concentration of DOX as well as its anticancer effect. In addition, the autophagic effect triggered by ZIF-8 promotes the degradation of ZIF-8, generating the release of cytotoxic Zn2+ and ROS, and the released Zn2+ in turn promotes autophagy, as well as doxorubicin-induced autophagy.[57] Liang et al reported that ZIF-8-based drug delivery system BSA/DOX@ZIF had a better effect on breast cells than free DOX did.[28] Chen et al encapsulated Fe_3O_4 in ZIF-8 loaded DOX, which was superior to DOX alone in in vitro experiments for the treatment of hepatocellular carcinoma.[47]

The present results established that Fe_3O_4-ZIF-8 enhanced DOX anti-tumorigenic effects and DFZ drug-loaded nanoparticles had higher efficacy than free DOX on K7M2 cells, DOX-loaded core-shell Fe_3O_4-ZIF-8 nanoparticles could have applications in osteosarcoma therapy.

Tumor Targeting Study

Tumor-targeting experiments of drug-carrying nanoparticles DFZ were performed in BALB/c tumor-bearing mice. In short, the Fe_3O_4@ZIF-8 nanocarrier was labeled with FAM and injected into mice via the tail vein. The fluorescence distribution in the mice was observed using small-animal in vivo imaging (Perkin Elmer, USA) with an applied magnetic field supplied by a permanent magnet. As exhibited in Figure 4A, regarding mice with an applied magnetic field, stable fluorescence was observed at the tumor site and remained relatively stable over 48 h. In contrast, mice without an applied magnetic field displayed almost no fluorescence at the tumor site at 48 h, Notably, there was also relatively strong fluorescence of tumor tissue in the magnet-free group, indicating the tumor EPR effect of magnetic nanoparticles DFZ. Eventually, the fluorescence intensity progressively decreased and was not detected after 48 h. Mice in both groups were euthanized 48 h after drug injection, and tumor tissues and other major organs were harvested for off-site tissue fluorescence imaging (Figure 4B), the fluorescence intensity of liver tissue was the highest among all tissues, and the fluorescence intensity of tumor tissue of mice

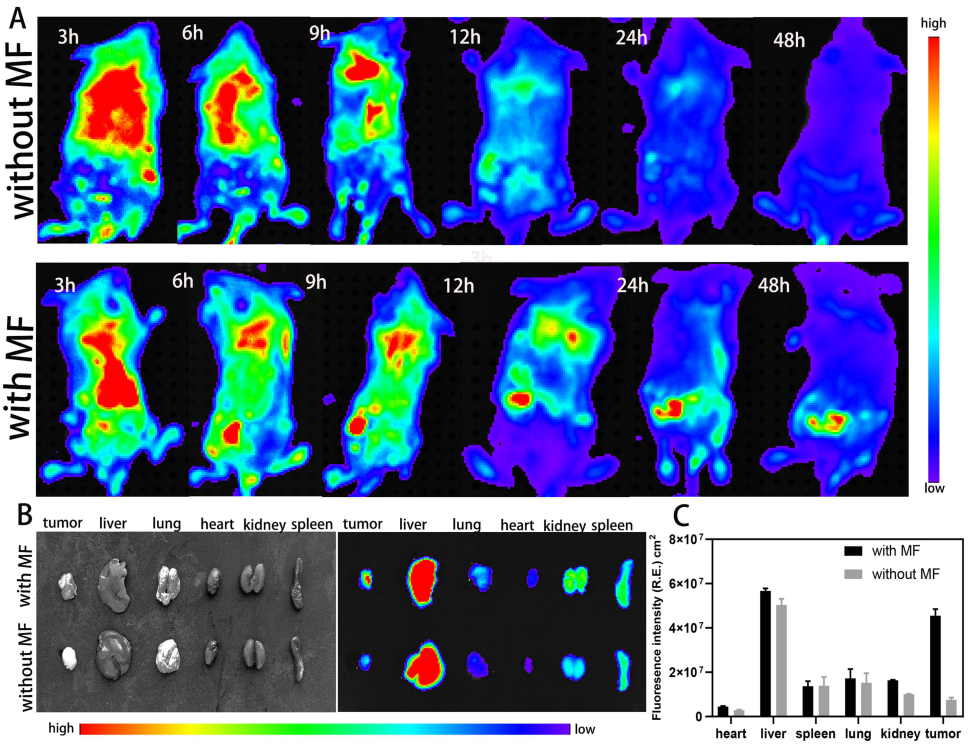

Figure 4 Tumor targeting of DFZ. (**A**) Whole-body fluorescence imaging of BALB/c mice after the injection of FAM labeled DFZ with/without external magnetic field. (**B** and **C**) Fluorescence intensity and quantitative analysis of tumor tissues and major organs in mice after 48 hours with/without external magnetic field, Error bars indicate the SD (n = 5).

subjected to DFZ with MF presented significantly higher tumor fluorescence signals than those not subjected to MF. Quantitative results uncovered that the fluorescence intensity of tumors treated with MF was approximately 6-fold higher than without MF (Figure 4C). Wang et al designed exosomes with iron oxide core and loaded with chemotherapeutic drugs, and the efficacy of the drug efficacy was enhanced by the action of magnetic guidance.[58] Similarly, the report on the use of iron oxide magnetic targeting in combination with other therapies also supports the effect of excellent active targeting,[59,60] These results demonstrated that DFZ is an efficient and active drug-carrying nanomaterial for magnetic targeting.

In vivo Anti-Tumor Study

We further investigated whether DFZ could treat mice with subcutaneous hamartomas. Antitumor experiments were performed in loaded mice with subcutaneous tumors up to 50 mm^3 in volume. The anti-tumorigenic effect was initially assessed by the change in tumor volume in mice. As demonstrated in Figure 5C, within 28 days, the tumor volume of mice in the G1 and G2 groups was significantly increased, suggesting that the Fe_3O_4@ZIF-8 nanocarrier did not exert an antitumor effect. On the other hand, mice in the G3-G5 groups showed a tumor inhibitory effect, all three were significantly different compared to G1. ($p < 0.01$), Tumor volume size was reduced in the G5 group by 83.22%. In other words, the tumor inhibitory effect of the applied magnetic field was higher in the DFZ group compared to the free DOX (41.63%) and DFZ groups without an applied magnetic field (61.88%). The tumor inhibition rate of DFZ was 1.5 times higher than that of the free drug combination (free DOX). The above results are consistent with the tumor weight and volume at the end of the experiment (Figure 5E and F), which can be explained by the enhanced drug accumulation retention at the tumor site and the accelerated drug release at the acidic tumor microenvironment.[39,54]

To further investigate the antitumor efficacy of the end of the treatment, we took a picture of solid tumors, which is illustrated in Figure 5D. As can be seen from their appearance, the G5 group has the smallest tumor volume. Furthermore, hematoxylin and eosin staining (H&E) were conducted on mice's tumor tissues (Figure 5A) to explore the anti-tumorigenic effect of DFZ. There were no signs of hemorrhagic necrosis in the tumor tissues and organs of mice

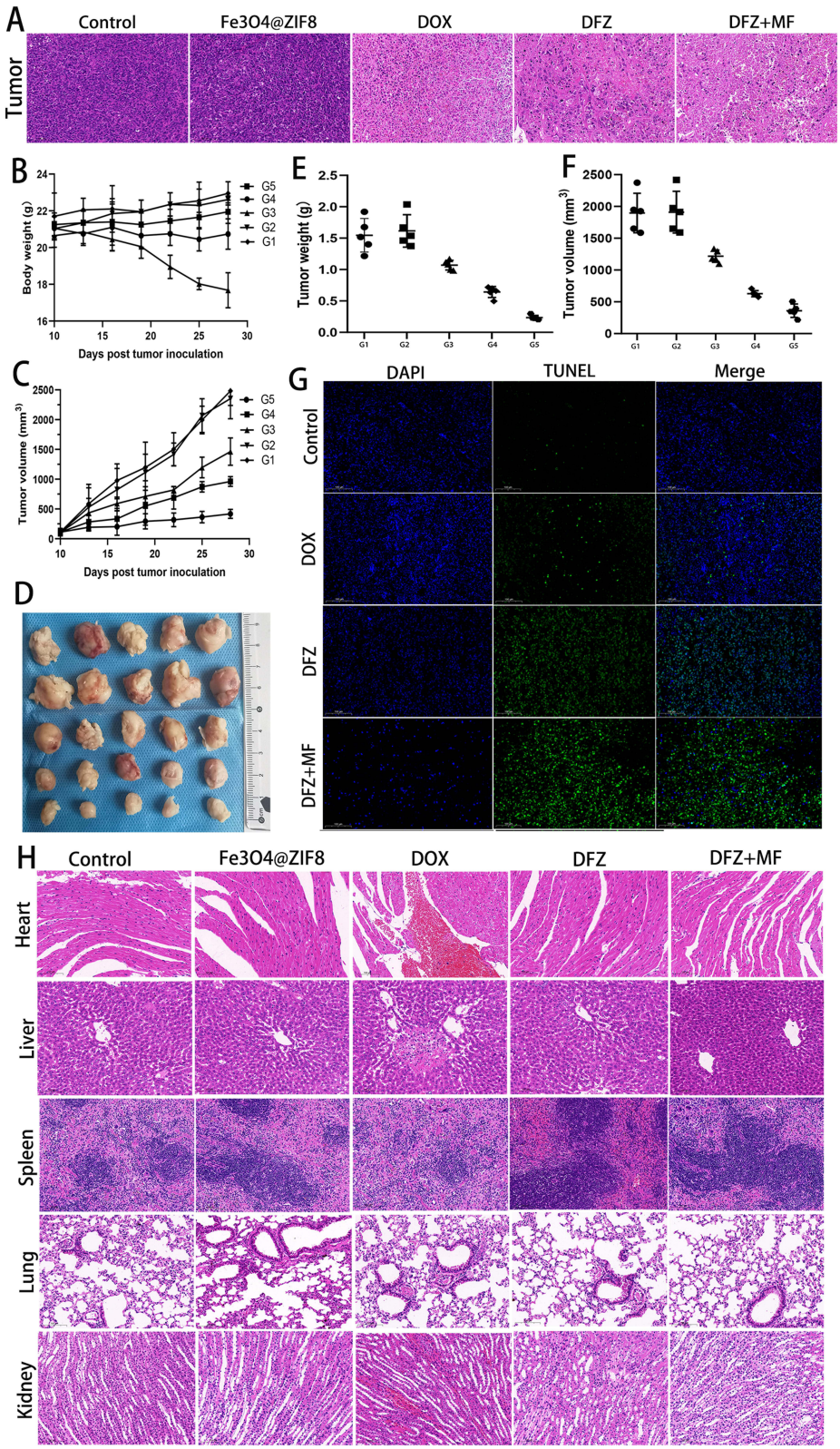

Figure 5 Antitumor effect of DFZ. (**A and H**) The H&E is staining images of the tumor and normal organs from mice after treatment with saline as control (G1), Fe_3O_4@ZIF-8 (G2), free DOX (G3), DFZ (G4), and DFZ+MF (G5). (**B and C**) Body weight and Tumor volume changes in the mice after treatment. Error bars indicate the SD (n = 5). (**D**) An image of the tumor at the end of the experiment. (**E**) Weight, and (**F**) Volume of tumor tissue. (**G**) Immunohistochemical (TUNEL) analyses of tumor tissue sections from mice treated with DFZ and processed with /without magnetic field. The statistical data are represented as the mean ± SD.

in the saline control and nanocarrier groups (Figure 5A). Conversely, cellular necrosis was detected in the tumor tissues of mice in the free DOX group, but the cell distribution remained compact. Significant areas of cellular necrosis were detected in tumors of both the G4 group and the G5 group, whereas the degree of hemorrhagic necrosis was higher in tumor tissues of mice in the G5 group.

Lastly, the next step was to evaluate apoptosis in the tumor tissues, which was accomplished by using TUNEL (Figure 5G). As shown in Figure 5G, the strongest and weakest fluorescence intensities occurred in the G1 and G5 groups, showing the fastest and slowest cell proliferation rates of osteosarcoma. Additionally, tumor tissue treated by DFZ with a magnetic field(G5) shows a more higher apoptosis rate than tumor tissue treated without a magnetic field (G4). The results confirmed that the apoptotic rate was higher in tumor tissues of mice in the magnetic field-treated DFZ group, followed by the magnetic field-free DFZ group. As anticipated, both groups had superior therapeutic outcomes compared to applying chemotherapeutic agents alone(G3). The results confirmed the significant in vivo anti-tumor effect and the targeted therapy mediated by Fe_3O_4 nanoparticles in suppressing tumor growth of DFZ. Following the previously reported in vivo experiments of amorphous ZIF-8 loaded with 5-Fu to form aZIF-8/5-Fu nanosystems,[45] Xie et al developed the results of a phosphorylcholine-based zwitterionic copolymer coated ZIF-8 nano-drug (DOX@ZIF-8@P (MPC-co-C7A)).[42]

In this experiment, the side effects of the drug were accompanied by the weight of the mice. The weight change curves (Figure 5B) revealed no significant change in mice in the G1 and G2 groups. However, due to the side effects of DOX, mice in the G3 group presented significant weight loss, the results further highlight the high biosafety profile of the Fe_3O_4@ZIF-8 nanocarrier in vivo.

Simultaneously, the number of animals and observation time were limited, this may indicate that neither the nanocarriers Fe_3O_4@ZIF-8 nor the DFZ-loaded particles had significant side effects on the mice in Figure 5B, but it is also possible that the side effects were not adequately reflected in the changes in body weight. Therefore, histological analysis of major organs of five groups of mice was performed in this experiment. As shown in Figure 5H, as evidenced by the stained sections of the organs of mice in the DOX group showing large areas of hemorrhage in heart and kidney tissues, as well as hepatic injury. Mice in the G4 and G5 groups had mild weight change. Still, there was no significant damage to the liver and essential organs, which validated that drug-carrying nanoparticles DFZ have a relatively substantial biosafety profile.

Thus, these results provide compelling evidence that the DFZ is a key factor in the achievement of a higher level of chemotherapeutic performance than a single treatment way.

Conclusion

Herein, the Fe_3O_4@ZIF-8 nanocarrier and drug-loaded nanoparticles DFZ composed of DOX were pioneered. The results successfully demonstrated that the Fe_3O_4@ZIF-8 nanocarrier and magnetic nanoparticles DFZ complex possessed the right particle size and a good capacity to carry the active ingredient via TEM, SEM, XRD, FT-IR, and Malvern Nano characterization techniques. This drug-loaded particle can be engulfed by osteosarcoma cells, is pH-responsive, and exhibits stable release characteristics in drug-release experiments. Additionally, the addition of ZIF material changes the mode of action of loaded drugs, it showed superior tumor cell inhibition and killing effect compared to DOX alone in vitro anti-tumor and apoptosis assays. Therefore, similar to vector Folic Acid-Carbon(FA-CD) loaded DOX for breast cancer,[61] targeted antitumor therapy with exosomal membrane protein encapsulated DOX,[62] and cisplatin (CDDP)-cross-linked hyaluronic acid (HA) nano gel delivery of DOX for osteosarcoma,[10] and Exo-DOX- Fe_3O_4@PDA-MB, which is an exosome-based platform with targeting and biocompatibility combined with chemical/genetic/photothermal therapy.[58] Thus, it is reasonable to speculate that DFZ can be used for the treatment of osteosarcoma. Obviously, in vitro, experiments to further apply DFZ to other cell lines have not yet been performed. In accordance with the animal experiments, the magnetic properties of the DFZ nanocomposites prepared in this experiment, which play a role in target localization as well as targeted therapy under the guidance of an applied magnetic field, also show good biocompatibility and anti-cancer ability in the application of DFZ alone. Guan et al fabricated bifunctional platform Fe_3O_4@SiO2-CDs magnetic nanoparticles loaded with the drug gambogic acid (GA), which had a more pronounced therapeutic inhibitory

effect in magnetically targeted in vivo experiments.[46] In addition, relying on the properties of ZIF materials, in the application of DFZ alone is also can show lower drug side effects and good anti-cancer ability in vitro.[45]

Thus, the above experimental results confirmed the potential of DFZ magnetic drug-carrying nanoparticles in circumventing the organ toxicity caused by large quantities of multiple chemotherapeutic doses as well as in enhancing the efficacy of chemotherapeutic drugs.

Animal Ethics Statement

BALB/c mice were provided by the Animal Experiment Center of Qingdao University. The study in vivo was performed under protocols approved by the Animal Management Rules of the Ministry of Health of the People's Republic of China (document No. 552001) and the examination and approval of the Laboratory Animal Welfare Ethics Committee of Qingdao University (ethical approval number: 20230709BALB/C350812077).

Acknowledgments

This work was funded by the Young Taishan Scholars Program(tsqn201909190); National Natural Science Foundation of China (82172478;82200440); Shandong Higher Education Young Science and Technology Support Program (2021KJ048;2023KJM003); Postdoctoral Science Foundation of China(2022T150340;2021M701813); Qingdao Postdoctoral Applied Research Project (2020); Innovation Fund of National Orthopedics and Sports Rehabilitation Clinical Medicine Research Center(2021-NCRC-CXJJ-ZH-02); Youth Talent Assistance Program of Medical College, Qingdao university. We thank the Home for Researchers editorial team (www.home-for-researchers.com) for the language editing service.

Disclosure

The authors report no conflicts of interest in this work.

References

1. Marchandet L, Lallier M, Charrier C, Baud'huin M, Ory B, Lamoureux F. Mechanisms of Resistance to Conventional Therapies for Osteosarcoma. *Cancers*. 2021;13(4):683. doi:10.3390/cancers13040683
2. Smrke A, Anderson PM, Gulia A, Gennatas S, Huang PH, Jones RL. Future Directions in the Treatment of Osteosarcoma. *Cells*. 2021;10(1):172. doi:10.3390/cells10010172
3. Gill J, Ahluwalia MK, Geller D, Gorlick R. New targets and approaches in osteosarcoma. *Pharmacol Ther*. 2013;137(1):89–99. doi:10.1016/j.pharmthera.2012.09.003
4. Chou AJ, Gorlick R. Chemotherapy resistance in osteosarcoma: current challenges and future directions. *Expert Rev Anticancer Ther*. 2006;6(7):1075–1085. doi:10.1586/14737140.6.7.1075
5. Gorlick R. Current concepts on the molecular biology of osteosarcoma. *Cancer Treatment Res*. 2009;152:467–478.
6. Harrison DJ, Geller DS, Gill JD, Lewis VO, Gorlick R. Current and future therapeutic approaches for osteosarcoma. *Expert Rev Anticancer Ther*. 2018;18(1):39–50. doi:10.1080/14737140.2018.1413939
7. Ferrari S, Serra M. An update on chemotherapy for osteosarcoma. *Exp Opinion Pharmacother*. 2015;16(18):2727–2736. doi:10.1517/14656566.2015.1102226
8. Carvalho C, Santos RX, Cardoso S, et al. Doxorubicin: the good, the bad and the ugly effect. *Curr Med Chem* 2009;16(25):3267–3285. doi:10.2174/092986709788803312
9. Mitchell MJ, Billingsley MM, Haley RM, Wechsler ME, Peppas NA, Langer R. Engineering precision nanoparticles for drug delivery. *Nat Rev Drug Discov*. 2021;20(2):101–124. doi:10.1038/s41573-020-0090-8
10. Zhang Y, Wang F, Li M, et al. Self-Stabilized Hyaluronate Nanogel for Intracellular Codelivery of Doxorubicin and Cisplatin to Osteosarcoma. *Adv Sci*. 2018;5(5):1700821. doi:10.1002/advs.201700821
11. Rahmani E, Pourmadadi M, Ghorbanian SA, Yazdian F, Rashedi H, Navaee M. Preparation of a pH-responsive chitosan-montmorillonite-nitrogen-doped carbon quantum dots nanocarrier for attenuating doxorubicin limitations in cancer therapy. *Eng Life Sci*. 2022;22(10):634–649. doi:10.1002/elsc.202200016
12. Wei H, Chen J, Wang S, et al. A Nanodrug Consisting Of Doxorubicin And Exosome Derived From Mesenchymal Stem Cells For Osteosarcoma Treatment In Vitro. *Int J Nanomed*. 2019;14:8603–8610. doi:10.2147/IJN.S218988
13. Feng Y, Gao Y, Wang D, Xu Z, Sun W, Ren P. Autophagy Inhibitor (LY294002) and 5-fluorouracil (5-FU) Combination-Based Nanoliposome for Enhanced Efficacy Against Esophageal Squamous Cell Carcinoma. *Nanoscale Res Lett*. 2018;13(1):325. doi:10.1186/s11671-018-2716-x
14. Wang X, Yang FF, Zhang LP, Huang YP, Liu ZS. A polyhedral oligomeric silsesquioxane/molecular sieve codoped molecularly imprinted polymer for gastroretentive drug-controlled release in vivo. *Biomater Sci*. 2018;6(12):3170–3177. doi:10.1039/C8BM01124A
15. Zhou ZF, Sun TW, Chen F, et al. Calcium phosphate-phosphorylated adenosine hybrid microspheres for anti-osteosarcoma drug delivery and osteogenic differentiation. *Biomaterials*. 2017;121:1–14. doi:10.1016/j.biomaterials.2016.12.031

16. Liu Y, Jiang Z, Tong S, et al. Acidity-Triggered Transformable Polypeptide Self-Assembly to Initiate Tumor-Specific Biomineralization. *Adv Materials*. 2023;35(15):56.
17. Chai Z, Hu X, Wei X, et al. A facile approach to functionalizing cell membrane-coated nanoparticles with neurotoxin-derived peptide for brain-targeted drug delivery. *J Controlled Release*. 2017;264:102–111. doi:10.1016/j.jconrel.2017.08.027
18. Wu MX, Yang YW. Metal-Organic Framework (MOF)-Based Drug/Cargo Delivery and Cancer Therapy. *Adv Materials*. 2017;29(23). doi:10.1002/adma.201606134
19. Ahmadi M, Ebrahimnia M, Shahbazi MA, Kecili R, Ghorbani-Bidkorbeh F. Microporous metal-organic frameworks: synthesis and applications. *J Ind Eng Chem*. 2022;115:1–11. doi:10.1016/j.jiec.2022.07.047
20. Yin M, Wu J, Deng M, et al. Multifunctional Magnesium Organic Framework-Based Microneedle Patch for Accelerating Diabetic Wound Healing. *ACS nano*. 2021;15(11):17842–17853. doi:10.1021/acsnano.1c06036
21. Qiao C, Zhang R, Wang Y, et al. Rabies Virus-Inspired Metal-Organic Frameworks (MOFs) for Targeted Imaging and Chemotherapy of Glioma. *Angewandte Chemie*. 2020;59(39):16982–16988. doi:10.1002/anie.202007474
22. Qiang S, Hu X, Li R, et al. CuS Nanoparticles-Loaded and Cisplatin Prodrug Conjugated Fe(III)-MOFs for MRI-Guided Combination of Chemotherapy and NIR-II Photothermal Therapy. *ACS Appl. Mater. Interfaces*. 2022;14(32):36503–36514. doi:10.1021/acsami.2c12727
23. Guo L, Zhong S, Liu P, Guo M, Ding J, Zhou W. Radicals Scavenging MOFs Enabling Targeting Delivery of siRNA for Rheumatoid Arthritis Therapy. *Small*. 2022;18(27):e2202604. doi:10.1002/smll.202202604
24. Huo Q, Liang Y, Lu W, et al. Integrated Metalloproteinase, pH and Glutathione Responsive Prodrug-Based Nanomedicine for Efficient Target Chemotherapy. *J Biomed Nanotechnol*. 2019;15(8):1673–1687. doi:10.1166/jbn.2019.2801
25. Cai W, Zhang W, Chen Z. Magnetic Fe(3)O(4)@ZIF-8 nanoparticles as a drug release vehicle: pH-sensitive release of norfloxacin and its antibacterial activity. *Colloids Surf B*. 2023;223:113170. doi:10.1016/j.colsurfb.2023.113170
26. Abdelhamid HN. Zeolitic Imidazolate Frameworks (ZIF-8) for Biomedical Applications: a Review. *Curr Med Chem*. 2021;28(34):7023–7075. doi:10.2174/0929867328666210608143703
27. Wang Q, Zhang Z, Qiu D, et al. LnNP@ZIF8 Smart System for In Situ NIR-II Ratiometric Imaging-Based Tumor Drug Resistance Evaluation. *Nanomaterials*. 2022;12(24):4478. doi:10.3390/nano12244478
28. Liang Z, Yang Z, Yuan H, et al. A protein@metal-organic framework nanocomposite for pH-triggered anticancer drug delivery. *Dalton Trans* 2018;47(30):10223–10228. doi:10.1039/C8DT01789A
29. Xuan S, Wang Y-XJ, Yu JC, Leung KC-F. Tuning the Grain Size and Particle Size of Superparamagnetic Fe3O4 Microparticles. *Chem Mater* 2009;21(21):5079–5087. doi:10.1021/cm901618m
30. Chen GH, Yu B, Lu CH, Zhang HH, Shen YQ, Cong HL. Controlled synthesis of Fe3O4@ZIF-8 nanoparticles for drug delivery. *Crystengcomm*. 2018;20(46):7486–7491. doi:10.1039/C8CE01302K
31. Wu Q, Wang D, Chen C, Peng C, Cai D, Wu Z. Fabrication of Fe3O4/ZIF-8 nanocomposite for simultaneous removal of copper and arsenic from water/soil/swine urine. *J Environ Manage*. 2021;290:112626. doi:10.1016/j.jenvman.2021.112626
32. Jiang X, Su S, Rao JT, et al. Magnetic metal-organic framework (Fe3O4@ZIF-8) core-shell composite for the efficient removal of Pb(II) and Cu(II) from water. *J Environ Chem Eng*. 2021;9(5):105959. doi:10.1016/j.jece.2021.105959
33. Huang X, Liu Y, Wang X, et al. Removal of Arsenic from Wastewater by Using Nano Fe(3)O(4)/Zinc Organic Frameworks. *Int J Environ Res Public Health*. 2022;19(17):85.
34. Al-Hazmi GH, Adam AMA, El-Desouky MG, El-Bindary AA, Alsuhaibani AM, Refat MS. Efficient Adsorption Of Rhodamine B Using A Composite Of Fe3o4@Zif-8: synthesis, Characterization, Modeling Analysis, Statistical Physics And Mechanism Of Interaction. *Bull Chem Soc Ethiop* 2023;37(1):211–229. doi:10.4314/bcse.v37i1.17
35. Esfahanian M, Ghasemzadeh MA, Razavian SMH. Synthesis, identification and application of the novel metal-organic framework Fe(3)O(4)@PAA@ZIF-8 for the drug delivery of ciprofloxacin and investigation of antibacterial activity. *Artif Cells Nanomed Biotechnol* 2019;47(1):2024–2030. doi:10.1080/21691401.2019.1617729
36. Wang P, Wang GY, Tang HW, et al. Preparation of Ropivacaine Encapsulated by Zeolite Imidazole Framework Microspheres as Sustained-Release System and Efficacy Evaluation. *Chemistry*. 2023.
37. Zhang M, Gao YY, Han LM, Zhu N, Gao XC. The construction of a multifunctional metal-organic framework for targeting tumors and bioimaging. *New J Chem*. 2020;44(42):18303–18307. doi:10.1039/D0NJ04463F
38. Schejn A, Mazet T, Falk V, et al. Fe3O4@ZIF-8: magnetically recoverable catalysts by loading Fe3O4 nanoparticles inside a zinc imidazolate framework. *Dalton Trans*. 2015;44(22):10136–10140. doi:10.1039/C5DT01191D
39. Sun CY, Qin C, Wang XL, et al. Zeolitic Imidazolate framework-8 as efficient pH-sensitive drug delivery vehicle. *Dalton Trans*. 2012;41(23):6906–6909. doi:10.1039/c2dt30357d
40. Zhang XM, Jiang JH, Yu QH, et al. ZIF-based carbon dots with lysosome-Golgi transport property as visualization platform for deep tumour therapy via hierarchical size/charge dual-transform and transcytosis. *Nanoscale*. 2022;14(23):8510–8524. doi:10.1039/D2NR02134J
41. Li M, Yue XF, Wang Y, Zhang J, Kan LW, Jing ZW. Remodeling the tumor microenvironment to improve drug permeation and antitumor effects by co-delivering quercetin and doxorubicin. *J Mat Chem B*. 2019;7(47):7619–7626. doi:10.1039/C9TB02131K
42. Xie RH, Yang P, Peng SJ, et al. A phosphorylcholine-based zwitterionic copolymer coated ZIF-8 nanodrug with a long circulation time and charged conversion for enhanced chemotherapy. *J Mat Chem B*. 2020;8(28):6128–6138. doi:10.1039/D0TB00193G
43. Lin Y, Zhong Y, Chen Y, et al. Ligand-Modified Erythrocyte Membrane-Cloaked Metal-Organic Framework Nanoparticles for Targeted Antitumor Therapy. *Mol Pharmaceut*. 2020;17(9):3328–3341. doi:10.1021/acs.molpharmaceut.0c00421
44. Li JH, Zhu DM, Ma WJ, et al. Rapid synthesis of a Bi@ZIF-8 composite nanomaterial as a near-infrared-II (NIR-II) photothermal agent for the low-temperature photothermal therapy of hepatocellular carcinoma. *Nanoscale*. 2020;12(32):17064–17073. doi:10.1039/D0NR03907A
45. Jiang Z, Li Y, Wei Z, et al. Pressure-induced amorphous zeolitic imidazole frameworks with reduced toxicity and increased tumor accumulation improves therapeutic efficacy In vivo. *Bioact Mater*. 2021;6(3):740–748. doi:10.1016/j.bioactmat.2020.08.036
46. Guan YX, Yang YX, Wang XX, et al. Multifunctional Fe_3O_4@SiO_2-CDs magnetic fluorescent nanoparticles as effective carrier of gambogic acid for inhibiting VX2 tumor cells. *J Mol Liq*. 2021;327.
47. Cheng C, Li C, Zhu X, Han W, Li J, Lv Y. Doxorubicin-loaded Fe(3)O(4)-ZIF-8 nano-composites for hepatocellular carcinoma therapy. *J Biomaterials Appl*. 2019;33(10):1373–1381. doi:10.1177/0885328219836540

48. Chen XR, Shi ZQ, Tong RL, et al. Derivative of Epigallocatechin-3-gallatea Encapsulated in ZIF-8 with Polyethylene Glycol-Folic Acid Modification for Target and pH-Responsive Drug Release in Anticancer Research. *ACS Biomater Sci Eng*. 2018;4(12):4183–4192. doi:10.1021/acsbiomaterials.8b00840
49. Shi Y, van der Meel R, Chen X, Lammers T. The EPR effect and beyond: strategies to improve tumor targeting and cancer nanomedicine treatment efficacy. *Theranostics*. 2020;10(17):7921–7924. doi:10.7150/thno.49577
50. Fang J, Islam W, Maeda H. Exploiting the dynamics of the EPR effect and strategies to improve the therapeutic effects of nanomedicines by using EPR effect enhancers. *Adv Drug Delivery Rev* 2020;157:142–160. doi:10.1016/j.addr.2020.06.005
51. Kent CA, Mehl BP, Ma L, Papanikolas JM, Meyer TJ, Lin W. Energy transfer dynamics in metal-organic frameworks. *J Am Chem Soc*. 2010;132(37):12767–12769. doi:10.1021/ja102804s
52. Avci C, Ariñez-Soriano J, Carné-Sánchez A, et al. Post-Synthetic Anisotropic Wet-Chemical Etching of Colloidal Sodalite ZIF Crystals. *Angewandte Chemie*. 2015;54(48):14417–14421. doi:10.1002/anie.201507588
53. Padhye P, Alam A, Ghorai S, Chattopadhyay S, Poddar P. Doxorubicin-conjugated β-NaYF4:Gd(3+)/Tb(3+) multifunctional, phosphor nanorods: a multi-modal, luminescent, magnetic probe for simultaneous optical and magnetic resonance imaging and an excellent pH-triggered anti-cancer drug delivery nanovehicle. *Nanoscale*. 2015;7(46):19501–19518. doi:10.1039/C5NR04473A
54. Adhikari C, Das A, Chakraborty A. Zeolitic Imidazole Framework (ZIF) Nanospheres for Easy Encapsulation and Controlled Release of an Anticancer Drug Doxorubicin under Different External Stimuli: a Way toward Smart Drug Delivery System. *Mol Pharmaceut*. 2015;12(9):3158–3166. doi:10.1021/acs.molpharmaceut.5b00043
55. Li X, Hou S, Chen J, et al. Engineering silk sericin decorated zeolitic imidazolate framework-8 nanoplatform to enhance chemotherapy. *Colloids Surf B*. 2021;200:111594. doi:10.1016/j.colsurfb.2021.111594
56. Wang Z, Niu J, Zhao C, Wang X, Ren J, Qu X. A Bimetallic Metal-Organic Framework Encapsulated with DNAzyme for Intracellular Drug Synthesis and Self-Sufficient Gene Therapy. *Angewandte Chemie*. 2021;60(22):12431–12437. doi:10.1002/anie.202016442
57. Xu M, Hu Y, Ding W, et al. Rationally designed rapamycin-encapsulated ZIF-8 nanosystem for overcoming chemotherapy resistance. *Biomaterials*. 2020;258:120308. doi:10.1016/j.biomaterials.2020.120308
58. Wang J, Chen P, Dong Y, et al. Designer exosomes enabling tumor targeted efficient chemo/gene/photothermal therapy. *Biomaterials*. 2021;276:121056. doi:10.1016/j.biomaterials.2021.121056
59. Sun XK, Dong B, Xu HW, et al. Amphiphilic Silane Modified Multifunctional Nanoparticles for Magnetically Targeted Photodynamic Therapy. *ACS Appl Mater Interfaces*. 2017;9(13):11451–11460. doi:10.1021/acsami.7b00647
60. Guo XM, Li W, Luo LH, et al. External Magnetic Field-Enhanced Chemo-Photothermal Combination Tumor Therapy via Iron Oxide Nanoparticles. *ACS Appl Mater Interfaces*. 2017;9(19):16581–16593. doi:10.1021/acsami.6b16513
61. Dada SN, Babanyinah GK, Tetteh MT, et al. Covalent and Noncovalent Loading of Doxorubicin by Folic Acid-Carbon Dot Nanoparticles for Cancer Theranostics. *ACS omega*. 2022;7(27):23322–23331. doi:10.1021/acsomega.2c01482
62. Tian Y, Li S, Song J, et al. A doxorubicin delivery platform using engineered natural membrane vesicle exosomes for targeted tumor therapy. *Biomaterials*. 2014;35(7):2383–2390. doi:10.1016/j.biomaterials.2013.11.083